Light-Induced Decoupling of Electronic and Magnetic Properties in Manganites

H. Navarro[1,*] Ali C. Basaran,[1] F. Ajejas,[1] L. Fratino,[2,3] S. Bag,[2] T.D. Wang,[1] E. Qiu,[1]
V. Rouco,[4] I. Tenreiro,[4] F. Torres,[5,6] A. Rivera-Calzada,[4] J. Santamaria,[4] M. Rozenberg,[2] and
Ivan K. Schuller[1]

[1] *Department of Physics, Center for Advanced Nanoscience, University of California, San Diego 92093, USA*

[2] *Université Paris-Saclay, Centre National de la Recherche Scientifique Laboratoire de Physique des Solides,
Orsay 91405, France*

[3] *Laboratoire de Physique Théorique et Modélisation, CNRS UMR 8089, CY Cergy Paris Université,
Cergy-Pontoise Cedex 95302, France*

[4] *Departamento de Física de Materiales, Universidad Complutense de Madrid, Madrid 28040, Spain*

[5] *Department of Physics, Universidad de Chile, Santiago 7800024, Chile*

[6] *Center for the Development of Nanoscience and Nanotechnology, CEDENNA, Santiago 9170124, Chile*

The strongly correlated material $La_{0.7}Sr_{0.3}MnO_3$ (LSMO) exhibits metal-to-insulator and magnetic transition near room temperature. Although the physical properties of LSMO can be manipulated by strain, chemical doping, temperature, or magnetic field, they often require large external stimuli. To include additional flexibility and tunability, we developed a hybrid optoelectronic heterostructure that uses photocarrier injection from cadmium sulfide (CdS) to an LSMO layer to change its electrical conductivity. LSMO exhibits no significant optical response; however, the CdS/LSMO heterostructures show an enhanced conductivity, with a resistance drop of about 37%, at the transition temperature under light stimuli. This enhanced conductivity in response to light is comparable to the effect of a 9 T magnetic field in pure LSMO. Surprisingly, the optical and magnetic responses of CdS/LSMO heterostructures are decoupled and exhibit different effects when both stimuli are applied. This unexpected behavior shows that heterostructuring strongly correlated oxides may require a new understanding of the coupling of physical properties across the transitions and provide the means to implement new functionalities.

I. INTRODUCTION

Strongly correlated electron systems display various physical phenomena such as superconductivity, ferroelectricity, ferromagnetism, and antiferromagnetism as a consequence of the intertwining of several degrees of freedom (charge, spin, strain, doping), producing a wide variety of phases and resulting in complex phase diagrams [1–6]. The critical response of these materials to a modification of the parameters makes them promising candidates for the next generation of electronic devices [7–12]. However, many of these variables are determined by intrinsic material properties set during growth and cannot be easily controlled in applications. Additional functionalities can be introduced by postgrowth modifications [8,13] or by interfacing the correlated oxides with other functional materials with very high sensitivity to external stimuli, such as light [12,14–16].

Manganites are one of the paradigmatic examples of strongly correlated electronic materials, showing a characteristic magnetoresistive behavior [17,18]. In particular, $La_{0.7}Sr_{0.3}MnO_3$ (LSMO) is one of the most studied materials for spintronic applications [19–21] due to its unique ferromagnetic and half-metallic order up to 360 K. The physical properties of LSMO can be tuned by modifying the electrical, magnetic, strain, and lattice degrees of freedom [22–27]. While the magnetic and electronic properties of LSMO are correlated, in practice it is often inefficient to control one with the other. In addition, spatial and temporal control of temperature with a certain precision often requires complex architectures and is not energy efficient [9,28]. Although LSMO is not sensitive to light, some oxygen-deficient LSMO thin films exhibit a persistent increase in electrical conductivity after light illumination at low temperature [23]. Moreover, $LSMO/MAPbI_3$ heterostructures show a change in their magnetization with light illumination [22]. These results show the great potential of hybrid heterostructures enabling optical functionalities with LSMO in technological applications for advanced

*hnavarro@physics.ucsd.edu

044077-1

oxide electronics [12,14]. This motivates the search for new functionalities by using light to control the electrical and magnetic properties of strongly correlated materials.

Recently, we reported a large modulation of the metal-insulator transition (MIT) temperature (T_c), for both non-volatile and volatile resistive switching, of Mott insulators VO_2, V_2O_3 [15], and V_3O_5 [29] by incorporating them into a heterostructure with photoconductive CdS [30]. Thus, motivated by the expectation of emergent proximity-induced interfacial effects, we heterostructured LSMO with light-sensitive CdS. We found that the resistance in the insulating state drops significantly when these heterostructures are illuminated with visible light while the transition temperature (T_c) remains constant. The volatile change in the resistance upon illumination depends on the LSMO thickness, suggesting that this is an interface effect. On the other hand, contrary to the effect of light, while a magnetic field lowers the resistance it also shifts the transition temperature to higher temperatures. We propose a model where the density of charge carriers increases upon

light illumination, resulting in enhanced conductivity. Our results show a practical way to control the electronic properties of manganites with light while also suggesting a new way to understand the coupling between electronic and magnetic properties in these strongly correlated systems.

II. RESULTS

We measured the resistance versus temperature [$R(T)$] in multiple CdS/LSMO samples with different LSMO thicknesses as shown in the inset of Fig. 1(c). The results of the hybrid sample with 3.5-nm LSMO thickness are plotted in Fig. 1. Figure 1(a) shows the $R(T)$ of the heterostructure when in the dark and illuminated with visible light of different powers. For all measurements, the resistance as a function of temperature is nonhysteretic, as recorded for both warming and cooling branches. In the dark (green curve), the hybrid CdS/LSMO exhibits a metal-to-insulator transition at 280 K. This behavior is
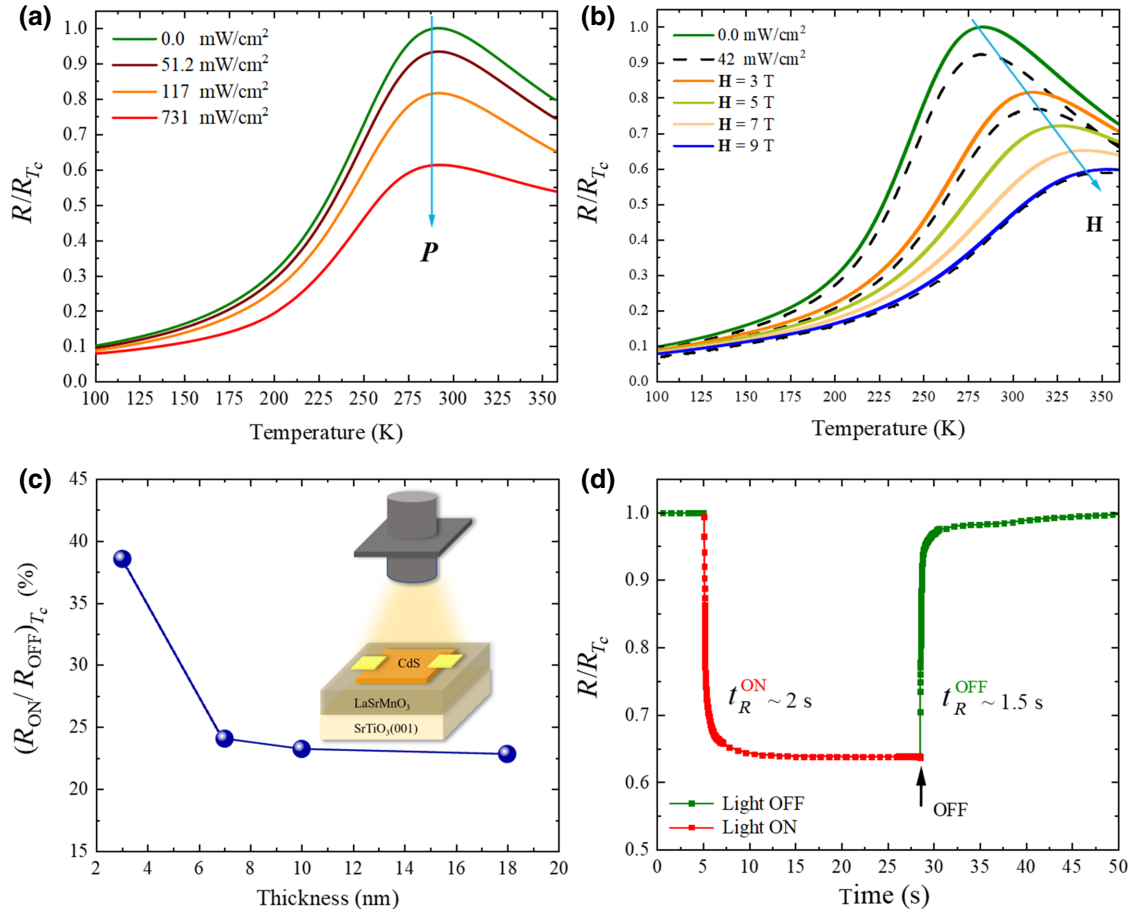

FIG. 1.   Light-induced modification of the metal-to-insulator transition in CdS/LSMO heterostructures. Resistance versus temperature $R(T)$ measurements for hybrid CdS/LSMO heterostructures, for (a) varying light power density and (b) varying magnetic field. The dashed lines in (b) shows the effect of 42-mW/cm^2 light for selected magnetic fields (0. 3, and 9 T). The solid green curves correspond to resistance versus temperature without light in all panels. (c) Change in the resistance at $T_c = 280$ K, with illumination for different LSMO thicknesses. (d) Relaxation of the resistance (normalized to resistance at $T_c = 280$ K).

expected from pure LSMO [31,32] and is in good agreement with the measured results of the control sample (pure LSMO thin film) shown in the Supplemental Material [37]. Such agreement confirms that the top CdS layer does not modify the LSMO electronic properties. With increasing light power density, the resistance of the insulating ground state decreases while the T_c (defined as the maximum in the resistivity versus T) remains constant [Fig. 1(a)]. The resistance drops more than 37% at T_c when the CdS/LSMO is exposed to a white light-emitting diode (LED) light with 731 mW/cm^2 illumination power density. In the absence of CdS, the effect of light on pure LSMO is negligible [Fig. S1(a) in the Supplemental Material [37]], which also indicates that heating effects are not significant.

Figure 1(b) shows the resistance versus temperature of the CdS/LSMO heterostructure (with 3.5-nm-thick LSMO) when an external magnetic field is applied (3–9 T). A larger applied magnetic field results in a more significant resistance drop. For instance, for $H = 3$ T, the resistance at T_c decreases by 20%, shifting the T_c of 23 K towards higher temperatures. This effect increases as the applied field increases, reaching a 40% resistance drop at T_c when a 9 T field is applied. Changes in T_c to higher temperatures are present for all applied fields. In Fig. 1(b) all solid lines are acquired in the dark. Interestingly, when the sample is subjected to both magnetic field and light (sequentially), the responses to the two stimuli are additive. The sample exhibits a shift of about 20 K in T_c, similar to the dark, but an additional 5% resistance drop still appears under illumination (represented by the dashed curves). However, the sample would cease to respond to light if a 9 T field were applied previously. Such behavior is shown in Fig. 1(b).

The percentage decrease of resistivity with light depends strongly on sample thickness: about 25% at 7 nm, 24%

at 10 nm, and 23% at 18 nm [Fig. 1(c)]. The absolute changes are shown in the Supplemental Material [37]. The decrease in the resistance change under the same illumination with increasing LSMO thickness indicates that this is an interfacial effect, which will be discussed later.

The relaxation time dependence of the CdS/LSMO resistance after light exposure is shown in Fig. 1(d). The change in the resistance before (green curve) and during illumination (red curve) at 280 K shows a decrease of 40% in less than 2 s. Once the minimum resistance is reached, the optical light source is turned off, recovering its original resistance in about 1.5 s. This shows that the effect of the light in the CdS/LSMO heterostructure resistance is volatile.

Figure 2 compares the effect of the two external stimuli, light and magnetic field, on the hybrid CdS/LSMO heterostructures. Figure 2(a) shows the normalized resistance drop $\Delta R/R_{T_c}$ at the transition temperature under illumination (solid red circles) and applied magnetic field (black squares). For both external stimuli cases, the resistance decreases with increasing amplitude. A light power density of $P = 731$ mW/cm^2 decreases the resistance by 40% at T_c, nearly the same as applying a very large 9 T external magnetic field.

To further compare the response of electrical properties to the two stimuli independently, Fig. 2(b) shows the dependence of T_c on each stimulus. Light illumination had negligible impact on T_c with a shift of 3 K at the maximum applied power density of 731 mW/cm^2. In contrast, the transition temperature increases linearly with the applied magnetic field. The T_c shift can be as large as 67 K when a 9 T external field is applied. This surprising result confirms the different origins of the two mechanisms.
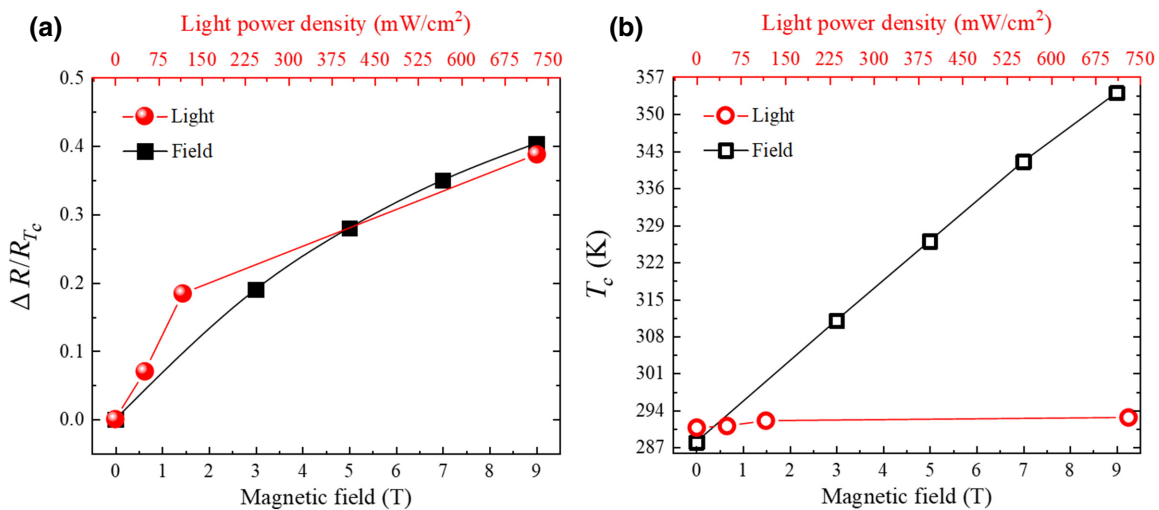

FIG. 2. Comparison between two external stimuli in hybrid CdS/LSMO heterostructure. (a) Normalized resistance changes ΔR at T_c as a function of applied magnetic field (black squares) and light power density (red circles). (b) T_c as a function of applied magnetic field (black open squares) and power density (red open circles).

The resistance decrease is expected to be driven by carrier injection from CdS to LSMO film. Similar to our previous report on CdS/VO$_x$ [29], the light response observed in CdS/LSMO is an interfacial effect between the CdS and LSMO layers. We observed that the response to light becomes smaller with LSMO layer thickness beyond 18 nm. However, in contrast to the present work, in the CdS/VO$_x$ case, light stimulation changes the resistance and the transition temperature together. This qualitative difference calls for a different physical model to explain the results found for CdS/LSMO.

Furthermore, when we subjected our sample to light while applying an external field [see Fig. 1(b)], the effect of light appears in the same way as without a field, namely, an increase in conductivity throughout the whole temperature range without a shift in transition temperature. However, when a larger field is applied, the light response becomes less pronounced. Below, we describe a model calculation to understand the cause of this behavior.

III. DISCUSSION

Generally, the electronic properties of La$_{1-x}$Sr$_x$MnO$_3$ may be described by the double exchange model [33,34]. Because of the Sr doping, the Mn atoms are in a mixed 3+/4+ valence state. Thus, three electrons of the 3d $t2g$ band form a "localized" spin-3/2 state at each site. On the other hand, there are $1 - x$ electrons per site occupying the conduction e_g band, therefore there are nominally x doped conduction hole carriers. The reason for this is the strong Hund's rule coupling. Thus, the conduction holes can be either strongly scattered or not by the localized 3/2 spins, depending on whether their spins are aligned antiparallel or parallel, respectively. Hence, when the core 3/2 spins are all aligned into a ferromagnetic state below T_c, the conduction electrons align to the direction of their magnetic moment m_z. In contrast, above the transition temperature, the core electrons are in a disordered paramagnetic state, and the conduction electrons suffer continuous scattering from the unavoidable misalignment of the spin moments. This explains qualitatively the MIT that characterizes the colossal magnetoresistance (CMR) manganites as they cross T_c.

We have incorporated these qualitative features in a phenomenological model to describe the results in the CdS/LSMO heterostructures. The density of conduction carriers is given by the doping x, which in the heterostructures is 0.3 per Mn site. Since the photoconductive CdS increases its number of free carriers upon illumination, we assume that part of the photoexcited carriers is transferred into the manganite thin film by a proximity effect. Thus, from the simple Drude model we have

$$\sigma = \frac{ne^2\tau}{m}, \tag{1}$$

where n is the carrier density, τ is average time between ionic collisions. Further assuming that the additional carrier density from the CdS, $n_0\Gamma$, is simply proportional to the illumination power, we have

$$n = n_0(1 + G), \tag{2}$$

and therefore, the resistivity is modulated by the effects of the light as:

$$\rho_\Gamma = \frac{\rho_0}{1 + \Gamma}, \tag{3}$$

To take into account the connection between magnetic behavior and resistivity, we adopt a slightly simplified version of the expression introduced by Wang *et al.* [35], which was motivated by the analysis of experimental data in terms of the double exchange model [33,34]:

$$\rho_0 = ATe^{(\epsilon(1-m_z^2))/T}, \tag{4}$$

where ε is the activation energy, T is the temperature, and A is a fitting parameter. The physical content of this formula is clear. At high $m_Z \sim 1$, deep in the ferromagnetic phase the exponent of this formula is small and a first-order expansion of the exponential, recovers the semiempirical form of the resistivity [31]. On the other hand, at small m_Z the resistivity crosses over to the activated form of a semiconductor.

The magnetization is governed by a ferromagnetic-paramagnetic transition at T_c. The effective coupling J between the local spins of Mn is related to the Hund's coupling J_H and the carrier number [31]. Since in LSMO at $x \sim 0.3$ the T_c depends weakly on x, we can take the parameter J as a constant [36]. Then, for simplicity, we model the temperature- and external field h-dependent FM transition by means of an Ising model solved in mean-field approximation:

$$m_z = \tan h\left(\frac{h + 4Jm_z}{T}\right), \tag{5}$$

which gives for the critical temperature $T_c = 4J$ at $h = 0$. We may now adopt suitable parameters for this model and explore its predictions.

Figure 3(a) shows the results from our model, including a decrease in the resistivity proportional to the applied light power without a shift in T_c, capturing the qualitative features of the experiment. As a further test of our model, we checked the effects of an external magnetic field h, as shown in Fig. 3(b). The magnetic field shifts the T_c to higher temperatures, also in good qualitative agreement with the experiments. The reason is that the external field provides further stability to the ferromagnetic phase. Thus, m_z survives at higher temperatures (see Supplemental Material Fig. S5 [37] for magnetization measurement
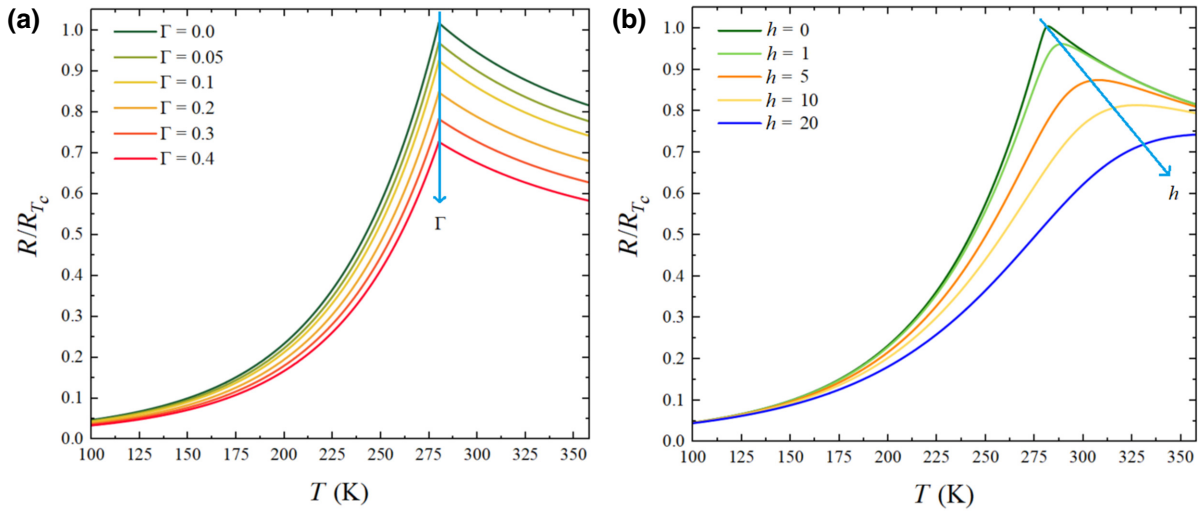
FIG. 3. Theoretically computed metal-insulator transition. (a) Change in the resistivity of LSMO as a function of temperature for different carrier densities Γ, (b) and for different applied fields, h.

as a function of thickness). Consequently, the maximum of the $\rho\ (T)$ that defines the MIT is shifted to higher temperatures.

IV. CONCLUSION

In conclusion, we demonstrated that the electronic conductivity of a hybrid optoelectronic CdS/LSMO heterostructure is modified by photocarrier injection from the CdS into the LSMO layer when exposed to light. Although the magnetic and electrical properties in pure LSMO are believed to be correlated, we can independently control the electrical and magnetic properties. While LSMO is known to have no significant optical response, our ultrathin film CdS/LSMO heterostructures show increased light-induced conductivity, with a resistance drop of about 37% at the transition temperature. The increase in conductivity with light is volatile and equivalent to applying a 9-T magnetic field in this colossal magnetoresistance material. Under a magnetic field, the transition moves to higher temperatures because of the increased stability of the ferromagnetic phase. The changes in the resistance under optical and/or magnetic stimuli are surprisingly independent of each other. Moreover, as the application of large magnetic fields is not readily achievable in most applications, our finding demonstrates an alternative practical way to control electronic properties with light in complex oxides.

V. EXPERIMENT

The ultrathin epitaxial LSMO samples (3.5, 7, 10, 18 nm) were grown on strontium titanate ($SrTiO_3$) $\langle 100 \rangle$ substrates using a high-pressure (3.2-mbar pure oxygen) and high-temperature (750 °C) sputtering. The target-to-substrate distance was set to 1.5 cm, so the highly confined

oxygen plasma was tangential to the substrate. CdS films 80 nm thick were grown in a separate deposition with rf magnetron sputtering from a CdS target in a 2-millitorr pure argon atmosphere at 150 °C. For each CdS/LSMO bilayer, two Au (40-nm) electrodes were patterned on the CdS/LSMO heterostructured films.

Morphological characterization measurements were performed in a Veeco scanning probe Microscope (SPM) by analyzing the topographic information in LSMO samples and CdS/LSMO heterostructures. The SPM images can be found in Supplemental Material Fig. S3 [37] for tapping mode. The structure of the films was analyzed by x-ray diffraction (XRD) in a Rigaku SmartLab system at room temperature (see Supplemental Material Fig. S4 [37] for structural characterization). Transport measurements were carried out on a Montana C2 S50 Cryocooler and TTPX Lakeshore cryogenic probe station, using a Keithley 6221 current source and a Keithley 2182A nanovoltmeter (see Supplemental Material Figs. S1 and S2 [37] for electrical transport measurements). A Thorlabs white LED was used for the photoconductivity measurements with a wavelength range of 400–700 nm. The magnetic characterizations and resistance measurements with applied field were performed in a Quantum Design DynaCool system equipped with a 9 T superconducting magnet, an optical probe, and a vibrating sample magnetometer.

[1] E. Dagotto, Complexity in strongly correlated electronic systems, Science **309**, 257 (2005).

[2] S. Kumari, N. Mottaghi, C.-Y. Huang, R. Trappen, G. Bhandari, S. Yousefi, G. Cabrera, M. S. Seehra, and M. B. Holcomb, Effects of oxygen modification on the structural and magnetic properties of highly epitaxial $La_{0.7}Sr_{0.3}MnO_3$ (LSMO) thin films, Sci. Rep. **10**, 3659 (2020).

[3] V. Strbik, M. Reiffers, E. Dobrocka, J. Soltys, M. Spankova, and S. Chromik, Epitaxial LSMO thin films with correlation of electrical and magnetic properties above 400 K, Appl. Surf. Sci. **312**, 212 (2014).

[4] F. Y. Bruno, J. Garcia-Barriocanal, M. Varela, N. M. Nemes, P. Thakur, J. C. Cezar, N. B. Brookes, A. Rivera-Calzada, M. Garcia-Hernandez, C. Leon, S. Okamoto, S. J. Pennycook, and J. Santamaria, Electronic and Magnetic Reconstructions in $La_{0.7}Sr_{0.3}MnO_3/SrTiO_3$ Heterostructures: A Case of Enhanced Interlayer Coupling Controlled by the Interface, Phys. Rev. Lett. **106**, 147205 (2011).

[5] R. Luo, X. Zhao, L. Chen, T. J. Legvold, H. Navarro, I. K. Schuller, and D. Natelson, Spin Seebeck effect at low temperatures in the nominally paramagnetic insulating state of vanadium dioxide, Appl. Phys. Lett. **121**, 102404 (2022).

[6] E. Qiu, P. Salev, L. Fratino, R. Rocco, H. Navarro, C. Adda, J. Li, M.-H. Lee, Y. Kalcheim, M. Rozenberg, and I. K. Schuller, Stochasticity in the synchronization of strongly coupled spiking oscillators, Appl. Phys. Lett. **122**, 094105 (2023).

[7] J. del Valle, P. Salev, F. Tesler, N. M. Vargas, Y. Kalcheim, P. Wang, J. Trastoy, M.-H. Lee, G. Kassabian, J. G. Ramírez, M. J. Rozenberg, and I. K. Schuller, Subthreshold firing in Mott nanodevices, Nature **569**, 388 (2019).

[8] P. Salev, J. del Valle, Y. Kalcheim, and I. K. Schuller, Giant nonvolatile resistive switching in a Mott oxide and ferroelectric hybrid, Proc. Natl. Acad. Sci. U.S.A. **116**, 8798 (2019).

[9] P. Salev, L. Fratino, D. Sasaki, R. Berkoun, J. del Valle, Y. Kalcheim, Y. Takamura, M. Rozenberg, and I. K. Schuller, Transverse barrier formation by electrical triggering of a metal-to-insulator transition, Nat. Commun. **12**, 5499 (2021).

[10] S. Cheng, M.-H. Lee, R. Tran, Y. Shi, X. Li, H. Navarro, C. Adda, Q. Meng, L.-Q. Chen, R. C. Dynes, S. P. Ong, I. K. Schuller, and Y. Zhu, Inherent stochasticity during insulator-metal transition in VO_2, Proc. Natl. Acad. Sci. U.S.A. **118**, e2105895118 (2021).

[11] R. Rocco, J. del Valle, H. Navarro, P. Salev, I. K. Schuller, and M. Rozenberg, Exponential Escape Rate of Filamentary Incubation in Mott Spiking Neurons, Phys. Rev. Appl. **17**, 024028 (2022).

[12] A. Rivera-Calzada, F. Gallego, Y. Kalcheim, P. Salev, J. del Valle, I. Tenreiro, C. León, J. Santamaría, and I. K. Schuller, Switchable optically active Schottky barrier in $La_{0.7}Sr_{0.3}MnO_3/BaTiO_3/ITO$ ferroelectric tunnel junction, Adv. Electron. Mater. **7**, 2100069 (2021).

[13] A. C. Basaran, C. Monton, J. Trastoy, R. Bernard, K. Bouzehouane, J. E. Villegas, and I. K. Schuller, Emergence of exchange bias and giant coercive field enhancement by internal magnetic frustration in $La_{0.67}Sr_{0.33}MnO_3$ thin films, J. Magn. Magn. Mater. **550**, 169077 (2022).

[14] I. Tenreiro, V. Rouco, G. Sánchez-Santolino, F. Gallego, C. Leon, A. Rivera-Calzada, I. K. Schuller, and J. Santamaria, Photovoltaic sensing of a memristor based in LSMO/BTO/ITO ferroionic tunnel junctions, Appl. Phys. Lett. **120**, 034101 (2022).

[15] H. Navarro, J.d. Valle, Y. Kalcheim, N. M. Vargas, C. Adda, M.-H. Lee, P. Lapa, A. Rivera-Calzada, I. A. Zaluzhnyy, E. Qiu, O. Shpyrko, M. Rozenberg, A. Frano, and I. K. Schuller, A hybrid optoelectronic Mott insulator, Appl. Phys. Lett. **118**, 141901 (2021).

[16] E. Di Gennaro, U. S. di Uccio, C. Aruta, C. Cantoni, A. Gadaleta, A. R. Lupini, D. Maccariello, D. Marré, I. Pallecchi, D. Paparo, P. Perna, M. Riaz, and F. M. Granozio, Persistent photoconductivity in 2D electron gases at different oxide interfaces, Adv. Opt. Mater. **1**, 834 (2013).

[17] Y. Tokura, Critical features of colossal magnetoresistive manganites, Rep. Prog. Phys. **69**, 797 (2006).

[18] P. K. Siwach, H. K. Singh, and O. N. Srivastava, Low field magnetotransport in manganites, J. Phys.: Condens. Matter **20**, 273201 (2008).

[19] J. H. Park, E. Vescovo, H. J. Kim, C. Kwon, R. Ramesh, and T. Venkatesan, Direct evidence for a half-metallic ferromagnet, Nature **392**, 794 (1998).

[20] J. Lloyd-Hughes, C. D. W. Mosley, S. P. P. Jones, M. R. Lees, A. Chen, Q. X. Jia, E. M. Choi, and J. L. MacManus-Driscoll, Colossal terahertz magnetoresistance at room temperature in epitaxial $La_{0.7}Sr_{0.3}MnO_3$ nanocomposites and single-phase thin films, Nano Lett. **17**, 2506 (2017).

[21] L. E. Hueso, J. M. Pruneda, V. Ferrari, G. Burnell, J. P. Valdés-Herrera, B. D. Simons, P. B. Littlewood, E. Artacho, A. Fert, and N. D. Mathur, Transformation of spin information into large electrical signals using carbon nanotubes, Nature **445**, 410 (2007).

[22] B. Náfrádi, P. Szirmai, M. Spina, A. Pisoni, X. Mettan, N. M. Nemes, L. Forró, and E. Horváth, Tuning ferromagnetism at room temperature by visible light, Proc. Natl. Acad. Sci. U.S.A. **117**, 6417 (2020).

[23] R. Cauro, A. Gilabert, J. P. Contour, R. Lyonnet, M. G. Medici, J. C. Grenet, C. Leighton, and I. K. Schuller, Persistent and transient photoconductivity in oxygen-deficient $La_{2/3}Sr_{1/3}MnO_{3-d}$ thin films, Phys. Rev. B **63**, 174423 (2001).

[24] X. Yin, C. S. Tang, M. A. Majidi, P. Ren, L. Wang, P. Yang, C. Diao, X. Yu, M. B. H. Breese, A. T. S. Wee, J. Wang, and

A. Rusydi, Modulation of manganite nanofilm properties mediated by strong influence of strontium titanate excitons, ACS Appl. Mater. Interfaces **10**, 35563 (2018).

[25] Z. Trajanovic, C. Kwon, M. C. Robson, K. C. Kim, M. Rajeswari, R. Ramesh, T. Venkatesan, S. E. Lofland, S. M. Bhagat, and D. Fork, Growth of colossal magnetoresistance thin films on silicon, Appl. Phys. Lett. **69**, 1005 (1996).

[26] S. K. Chaluvadi, F. Ajejas, P. Orgiani, O. Rousseau, G. Vinai, A. Y. Petrov, P. Torelli, A. Pautrat, J. Camarero, P. Perna, and L. Mechin, Room temperature biaxial magnetic anisotropy in $La_{0.67}Sr_{0.33}MnO_3$ thin films on $SrTiO_3$ buffered MgO (001) substrates for spintronic applications, Appl. Phys. Lett. **113**, 052403 (2018).

[27] P. Perna, D. Maccariello, F. Ajejas, R. Guerrero, L. Méchin, S. Flament, J. Santamaria, R. Miranda, and J. Camarero, Engineering large anisotropic magnetoresistance in $La_{0.7}Sr_{0.3}MnO_3$ films at room temperature, Adv. Funct. Mater. **27**, 1700664 (2017).

[28] F. Torres, A. C. Basaran, and I. K. Schuller, Thermal management in neuromorphic materials, devices, and networks, Adv. Mater., Accepted Author Manuscript, 2205098 (2022).

[29] C. Adda, H. Navarro, J. Kaur, M.-H. Lee, C. Chen, M. Rozenberg, S. P. Ong, and I. K. Schuller, An optoelectronic heterostructure for neuromorphic computing: CdS/V_3O_5, Appl. Phys. Lett. **121**, 041901 (2022).

[30] K. Deng and L. Li, CdS Nanoscale photodetectors, Adv. Mater. **26**, 2619 (2014).

[31] S. Jain, H. Sharma, A. Kumar Shukla, C. V. Tomy, V. R. Palkar, and A. Tulapurkar, Optimization of $La_{0.7}Sr_{0.3}MnO_3$ thin film by pulsed laser deposition for spin injection, Phys. B **448**, 103 (2014).

[32] Z. Liao, F. Li, P. Gao, L. Li, J. Guo, X. Pan, R. Jin, E. W. Plummer, and J. Zhang, Origin of the metal-insulator transition in ultrathin films of $La_{2/3}Sr_{1/3}MnO_3$, Phys. Rev. B **92**, 125123 (2015).

[33] C. Zener, Interaction between the d-shells in the transition metals. II. Ferromagnetic compounds of manganese with perovskite structure, Phys. Rev. **82**, 403 (1951).

[34] E. Dagotto, *Nanoscale phase separation and colossal magnetoresistance: The physics of manganites and related compounds* (Springer, Berlin, 2003), p. 71.

[35] J. Z. Wang, J. R. Sun, G. J. Liu, F. X. Hu, T. Y. Zhao, and B. G. Shen, A universal relation between resistivity and magnetization in paramagnetic state of manganites, Appl. Phys. Lett. **91**, 262506 (2007).

[36] H. Fujishiro, T. Fukase, and M. Ikebe, Charge ordering and sound velocity anomaly in $La_{1-x}Sr_xMnO_3$ ($X \geq 0.5$), J. Phys. Soc. Jpn. **67**, 2582 (1998).

[37] See Supplemental Material at http://link.aps.org/supplemental/10.1103/PhysRevApplied.19.044077 for additional data and analysis, including Figs. S1–S9.